Developing a relationship between static Young's modulus and seismic parameters

Javad Sharifi[1] · Mohammad Nooraiepour[2] · Mohammadkazem Amiri[3,5] · Nazmul Haque Mondol[2,4]

Abstract

Mechanical properties of petroleum reservoirs can be determined via static techniques based on laboratory triaxial tests under reservoir conditions. Dynamic approaches represent an alternative in cases where such static laboratory data are unavailable. Dynamic elastic properties are calculated using ultrasonic wave measurements in the laboratory or in situ well logging. Different relationships have been proposed to estimate static properties from dynamic ones based on the available data from a particular reservoir. However, these relationships are often reservoir-specific, making them inadequate for general seismic inversion purposes. This research proposes a method for developing relationships between seismic parameters and static Young's modulus in carbonate reservoirs by integrating ultrasonic measurements, well logging data, and rock mechanic tests. A multistage triaxial test simulating the reservoir conditions was used to fully control the stress and strain during the geomechanical experiments. Static Young's modulus was cross-correlated with a broad spectrum of seismic parameters that can be extracted from seismic inversion (e.g., acoustic impedance, shear impedance, Lambda–rho, and mu–rho). Separate analytic relationships were proposed to convert dynamic Young's modulus and seismic parameters into static Young's modulus. Analysis of variance was used to evaluate the results and study the applicability and reliability of the obtained relationships. Furthermore, the reliability of the obtained relationships was successfully confirmed by well logging data and blind well analysis. The proposed methodology can be used to predict rock behavior for geomechanical and structural modeling.

Keywords Static Young's modulus · Seismic parameters · Seismic–geomechanics inversion rock physics · Rock mechanics

Introduction

Investigation of mechanical properties of rocks and quantitative characterization of reservoir rocks is critical for exploration and production activities, such as well

✉ Javad Sharifi
J_sharifi@mail.um.ac.ir; Jv_sharifi@yahoo.com

1 Department of Geology, Faculty of Science, Ferdowsi University of Mashhad, P.O. Box 9177948974, Mashhad, Iran

2 Department of Geosciences, University of Oslo, P.O. Box 1047, Blindern, 0316 Oslo, Norway

3 Enhanced Oil Recovery (EOR) Research Centre, IOR/EOR Research Institute, Shiraz University, Shiraz, Iran

4 Norwegian Geotechnical Institute (NGI), P.O. Box 3930, Ullevaal Stadion, 0806 Oslo, Norway

5 Present Address: Petrogostaran Ofogh (PGO) Company, Ahvaz, Iran

completion, casing design, and development of proper drilling plan (Zoback 2010; Farrokhrouz et al. 2014; Kidambi and Kumar 2016; Zare-Reisabadi et al. 2018; Fjær 2019). Mechanical properties of rocks can be measured by static approaches or estimated by dynamic approaches when the former is not feasible. Static elastic moduli are determined through mechanical tests in the laboratory (e.g., triaxial deformation test), while the dynamic moduli can be estimated from acoustic wave velocities (ultrasonic or well logging). In recent years, integrating well logs and rock mechanics for estimating elastic parameters has been one of the most important developments in the geomechanical research, facilitating the geomechanical modeling (e.g., Lockner et al. 1991; Brotons et al. 2014; Najibi et al. 2015; Amiri et al. 2019b; Fjær 2019; Sharifi 2022). In this regard, the integration of geomechanics and seismic plays an essential role in estimating the stress field and mechanical properties of rocks across reservoir unit. It implies that the geomechanical parameters can be estimated from seismic

Fig. 1 Geography and geology maps of selected case study: **a** geological subdivisions map and **b** stratigraphic chart of the study area in SW Iran. Pink stars mark the study area and targeted stratigraphic horizon

data based on empirical relationships for dynamic-to-static conversion (Herwanger and Koutsabeloulis 2011; Gray et al. 2012; Jiang and Xiong 2019; Sharifi et al. 2019; Ugbor et al. 2021). As a widely applied and fundamental rock property, Young's modulus (E_s) is important for geomechanical reservoir characterization. This sheds lights on the significance of either measuring Young's modulus through static approaches or estimating it by dynamic approaches (dynamic Young's modulus; E_d) using compressional and shear-wave velocities (P- and S-wave) and density. Over the past 80 years, various empirical formulations have been proposed for estimating static Young's modulus from the wave velocity for different geological areas with different depositional settings (e.g., Ide 1936; Deere and Miller 1966; King 1983; Eissa and Kazi 1988; Petrov 2014; Fei et al. 2016; Sharifi et al. 2017; Fjær 2019). Hampson et al. (2005) presented a new approach to the pre-stack seismic inversion to obtain P-impedance, S-impedance, and density simultaneously. The goal of pre-stack seismic inversion is to estimate P- and S-wave velocities and bulk density from seismic data to predict the lithology and fluid properties in the subsurface. Currently, not much research has been published on dynamic-to-static conversion using seismic inversion results. This is while seismic parameters such as acoustic impedance (I_p), shear impedance (I_s), and LMR (lambda–rho; LR and mu–rho; MR) can be obtained from seismic inversion by deterministic or stochastic methods (Hampson et al. 2005; Sen 2006) and play vital roles in reservoir characterization. Therefore, significant inconsistencies could be found when dynamic-to-static relationships are used for obtaining geomechanical parameters from seismic inversion outputs. Developing specific relationships is hence necessary to use indirect conversion of acoustic and shear impedance to geomechanical parameters.

In this study, a total of 20 core samples taken from a 100 m reservoir interval in Ilam Formation (a carbonate formation in SW Iran) together with well logging data were investigated to develop relationships between the seismic inversion outputs (I_p, I_s, and LMR) and static Young's moduli. The obtained data were based on multistage triaxial tests and ultrasonic testing to study the parameters affecting the dynamic-to-static relationship. The selected core samples were tested under in situ conditions corresponding to 2.5–3.5 km burial depths. The experimental results were interpreted to develop seismic–geomechanics relationships. Different parameters were investigated to identify their impacts on the static-to-dynamic conversion. Finally, simple and multiple linear regressions were carried out to correlate the seismic parameters and static Young's moduli.

Geological setting

The study area is located in the Zagros Mountain Belt, southwestern Iran (Fig. 1). The mountain belt is located between the Arabian Plate and Eurasia (Iranian block) and follows an NW–SE trend. Dezful Embayment is part of the Zagros fold thrust belt (Motiei et al. 1993). A number of the most significant hydrocarbon reserves within the Zagros fold thrust belt and Arabian Platform have been developed in the Bangestan Group, a set of formations dated back to the Albian to Campanian. These formations within the Bangestan Group are mainly composed of neritic carbonates. Ilam Formation consists of light gray shallow marine limestone with black fossiliferous shale and is cut through by intra-formational
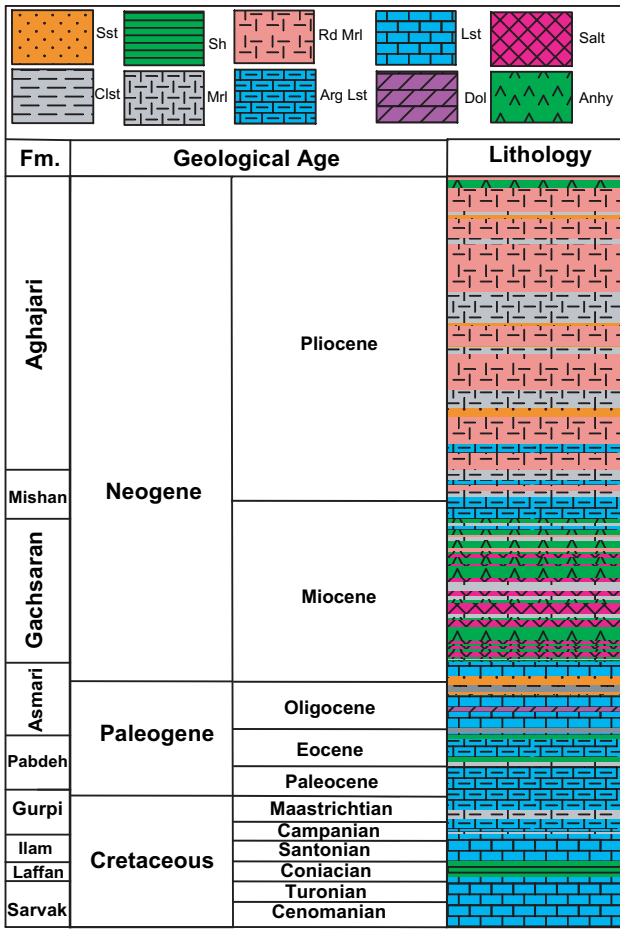
Fig. 2 Geological graphic well log display of well D-020. A stratigraphic column is also added to the figure. The Ilam and Sarvak Formations penetrated by the well are the main reservoirs in Dezful Embayment, SW Iran

to Campanian–Maastrichtian, composed of marls to marly limestones) and Laffan Formation (comprised mainly of Coniacian shales), as demonstrated in Fig. 1 (Motiei et al. 1993; Rajabi et al. 2010).

Data review

One of the wells in this area (Well No. D-020) was chosen for modeling in this study. The trajectory of the selected well was almost vertical; therefore, the measured depth was considered a true vertical depth. Figure 2 shows the graphic well log of drilled well, which presents geological formation and lithology. The well penetrated about 200 m of the reservoir thickness mainly into a brine column with some portions of heavy oil. In this area, as the reservoir of interest, Ilam Formation is approximately 190 m thick and extends along with a depth range of 2900–3090 m from mean sea level. A total of 100-m whole cores with a diameter of 150 mm were retrieved from Ilam intervals (2900–3000 m) at a core recovery ratio of 95%. A suite of well logs, including gamma-ray, P-wave (V_p), and S-wave (V_s) velocities, bulk density (RHOB), electrical resistivity, and neutron porosity (NPHI) were available for formation evaluation. The salinity and hydrocarbon properties, as well as in situ formation fluid pressure (30–35 MPa) and temperature (100–110 °C) were acquired through a well testing program (Drill Stem Test, DST). Formation total porosity was obtained from the NPHI and bulk density well logs (Fig. 4).

disconformities. The core samples were selected from the Ilam Formation (Santonian–Campanian) which is stratigraphically located between Gurpi Formation (dated back
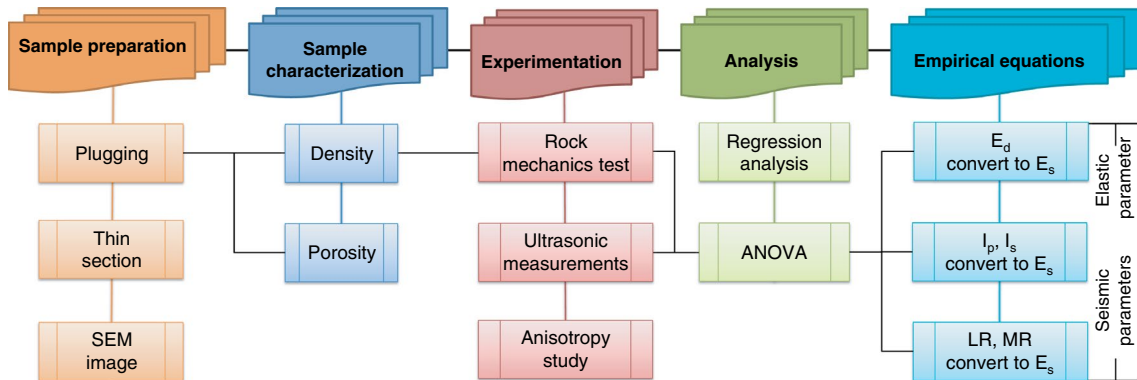

Fig. 3 Workflow of the proposed methodology. It starts with sample preparation and continues with sample characterization, rock mechanics experiments and rock physics tests (ultrasonic measurements).

Finally, it finishes with the development of empirical relationships between static Young's modulus (E_s) and dynamic Young's modulus (E_d) using particular seismic parameters (I_p, I_s, and LMR)
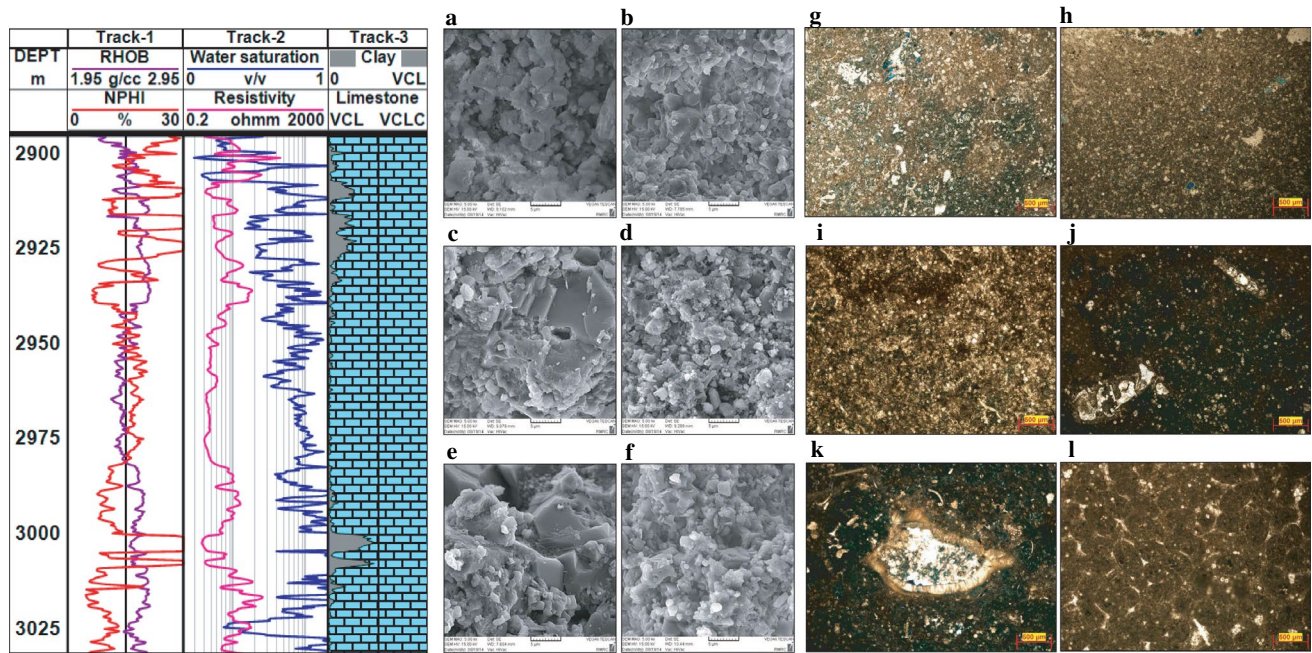
Fig. 4 Well logging data for a studied given well. Track 1 shows RHOB and NPHI, track 2 shows water saturation and resistivity on a logarithm scale, and track 3 shows the interpreted lithology. Scanning electron microscope (SEM) micrographs of each core sample are also shown: **a–f** 5-µm SEM images; **g–l** 500-µm images of thin sections. The grains are bound by a clay cement that is not spread in this formation

Methodology and experiments

The workflow of the present study is summarized in Fig. 3. This workflow starts with sample preparation and continues with sample characterization, experimentation, and analysis. Then, the research comes to a conclusion by proposing some empirical equations for converting dynamic Young's modulus to static Young's modulus, incorporating seismic parameters, core measurements, and well log data.

Sample preparation

In this research, 20 core plugs from a carbonate reservoir (Ilam Formation) were tested. These core samples were cut parallel to the drilling direction with a length ranging from 10 to 12 cm. Toluene and methanol were used to remove hydrocarbon and formation brine from the samples, respectively, in two separate steps. Subsequently, the plugs were dried in a conventional oven at 60 °C for one day. Next, the samples were saturated using a synthetic fluid (210,000 ppm NaCl). The salinity of the synthetic fluid was representative of the formation brine at the studied well. The saturation was achieved based on the methods described by Amalokwu et al. (2016). The prepared specimens were tested under reservoir conditions in

terms of saturation and temperature. To simulate reservoir conditions in the laboratory, such as pressure, poroelastic formulae were used to estimate in situ stress. In this regard, in situ horizontal and vertical stresses were calculated considering normal faulting regimes according to Anderson's (1951) classification scheme. In situ stress estimations suggest 1.35 MPa increase in the effective (vertical) stress per 100 m increase in the burial depth (Rajabi et al. 2010; Sharifi and Mirzakhanian 2018; Zare-Reisabadi et al. 2018).

Sample characterization

Sampling depths were accurately determined using gamma-ray measurements in the laboratory. For this purpose, the gamma spectrum and bulk density of the core samples were measured by a spectral gamma logger instrument. The microstructure of the samples was investigated using scanning electron microscopy (SEM) and thin section analyses (Fig. 4). For this purpose, two thin sections were taken from each plug (from the top and base of the horizontal and vertical plugs) and characterized in terms of facies, pore type, and depositional setting. To study bulk (whole–rock) and clay mineralogical composition, X-ray diffraction (XRD) analysis was performed on the core samples. The grain
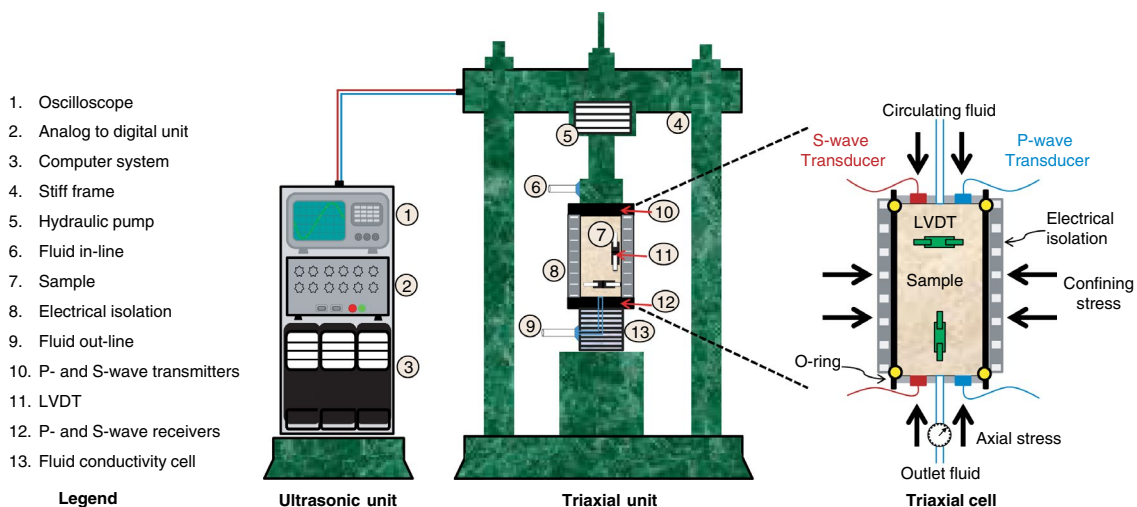
Fig. 5 Schematic of the triaxial loading frame, triaxial cell, and ultrasonic measurement unit. The system consists of a loading frame with a loading capacity of 450 kN and a 70-MPa test cell. Several internal electronic and hydraulic feed-through transducers were installed in the load cell (i.e., radial and axial displacement transducers) to record the deviatoric stress and pore pressures on both ends of the sample
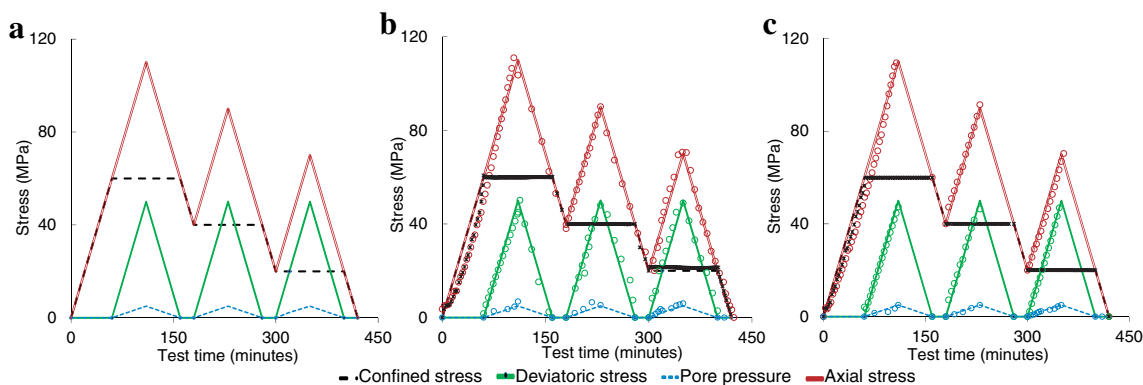

Fig. 6 Stress versus experimental elapsed time for two samples in this study: **a** schematic model, **b** sample No. 2, and **c** sample No. 5. The geomechanical experiments were conducted under drained conditions. Because of the low matrix permeability, only small pore pressure development was recorded during the test at peak axial stress

density and total porosity were measured using an Ultra Porosimeter via helium injection. Based on Boyle's law, the apparatus can evaluate pore or grain volume by expanding a specific helium mass into a calibrated sample holder.

Multistage triaxial test

The samples were subjected to multistage triaxial testing to obtain static parameters in this study. Experiments were conducted on a high-stiffness Autonomous Triaxial Cell (ATC) equipped with acoustic measurement transducers. Figure 5 presents a schematic of the experimental apparatus. The system was made up of a loading frame with a loading capacity of 450 kN, an actuator powered by a stepping motor pump, and a 70-MPa test cell. The sample holder had two diametrically opposed linear variable differential transformer (LVDT) displacement transducers for vertical strain and height change measurements.

The test specimen was mounted in the triaxial loading cell, where it was subjected to uniform hydrostatic loading at 0.5 MPa/min up to a predetermined confining pressure. Multistage tests were performed within the elastic region of the samples according to the ASTM standard (Kim and Ko 1979; Hashiba and Fukui 2014; Sharifi et al. 2017). Different confining pressures (60, 40, and then 20 MPa) were applied at the same deviatoric stress (50 MPa) in each stage (Fig. 6). Upon stabilization of the confining pressure in the first stage (at 60 MPa), the deviatoric load was increased to 50 MPa at a constant strain rate of 0.0005 1/min in the reservoir condition. Due to the applied deviatoric load, the axial stress

increased gradually to 110 MPa under drained conditions, and output fluid volume and pressure were recorded at the end of the sample. All tests were conducted under a strain-controlled condition. For each sample, the test was performed for about 450 min. Details of the loading schemes for the two samples are schematically demonstrated in Fig. 6. The same procedure was followed for other samples.

The axial stress versus strain curve slope gives the static Young's modulus. By definition, the E_t or tangent Young's modulus refers to the slope of the axial strain to the axial stress curve when the applied stress is 50% of the peak strength of the sample (Goodman 1989; Brady and Brown 2013). In this study, Young's modulus was represented by the tangent Young's modulus (E_t, in GPa).

Ultrasonic velocity measurement

Dynamic Young's modulus was calculated using well logs ($f = 10$–20 kHz) and laboratory measurements ($f = 500$–1000 kHz). The conventional pulse transmission technique was used on core samples in the laboratory to calculate P-wave and S-wave velocities at ultrasonic frequencies under reservoir conditions (Hamilton and Bachman 1982; McCann and Sothcott 1992; Mockovčiaková and Pandula 2003; Nooraiepour et al. 2017a). The experimental apparatus was equipped with piezoelectric transducers—one at its base plate to receive an ultrasonic wave and another one at its top cap to transmit the ultrasonic wave. An Acoustic Transducer Instrumentation Unit (ATIU) was used for acoustic signal switching and pinging/receiving with acoustic signal conditioning circuitry (Fig. 5, ultrasonic unit). The acoustic signal produced by the transducer was made up of P, S_1, and S_2 components. A shear (or flexural) wave generated by a dipole source can be split into two orthogonal components polarized along the x- and y-axes in the sample (or geological formation). Upon propagation through the sample, the first waves (x-axes) tend to be polarized in a direction parallel to the strike of the fracture, while the second waves (y-axes) propagate in the normal direction (Thomsen 1986; Brie et al. 1998). The shear-wave transducer used in this study could measure these two components: Vs_1 and Vs_2, in the test results. The largest errors in the velocity measurements are sourced from the arrival time determination from the raw waveform and the sample height measurement. For all samples, the estimated error of ultrasonic wave velocity measurement was calculated to range between 0.45 and 0.55% for V_p and 0.61% and 0.75% for V_s. Further velocity error analyses were performed according to Yin (1992) and Hornby (1998). After obtaining P- and S-wave velocities of rock samples, other elasticity parameters can be calculated as follows (Mavko et al. 2009):

$$v = \frac{(V_p/V_s)^2 - 2}{2\left[(V_p/V_s)^2 - 1\right]} \tag{1}$$

$$\mu = \rho V_s^2 \Rightarrow \text{MR} = \mu\rho \tag{2}$$

$$E_d = 2\mu(1 + v) \tag{3}$$

$$\lambda = \mu\frac{2v}{1 - 2v} \Rightarrow \text{LR} = \lambda\rho \tag{4}$$

$$I_p = \rho V_p \tag{5}$$

$$I_s = \rho V_s \tag{6}$$

where V_p and V_s are the P- and S-wave velocities, respectively, v and μ are the dynamic Poisson's ratio and shear modulus, respectively, while ρ indicates the density. Furthermore, E_d and λ are dynamic Young's modulus and Lame's coefficient, respectively, and I_p and I_s denote P- and S-impedance, respectively.

Anisotropy calculation

Sedimentary rocks exhibit anisotropy due to intrinsic heterogeneities and structural effects such as thin layering and unequal stresses within the formation or aligned fractures. Many anisotropic models have been proposed during the past decades. Among these, the transversely or hexagonally isotropic system seemed to suit the present research considering the available data (Serra 1986; Thomsen 1986; Mavko et al. 2009; Saberi and Ting 2016). Thomsen (1986) introduced three anisotropy parameters (ε, γ, and δ) to describe weak anisotropy, which is believed to be the simplest model of anisotropy. Dipole Shear Sonic Imager (DSI) is a tool for acquiring sonic measurements from formations surrounding a borehole. When propagating through a formation, a shear (or flexural) wave generated by a dipole source splits into two orthogonal components polarized along the x- and y-axes. Considering the availability of data and in order to quantify the anisotropy parameters in the weak anisotropy system encountered in this research, γ (gamma) constant was used. It describes the fractional difference between the S-wave velocities in the directions parallel and orthogonal to the axis of symmetry (Eq. 7). This was equivalent to the difference between the velocities of the S-waves polarized parallel and normal to the axis of symmetry and propagating normal to this axis.

$$\gamma = \frac{V_{SH}(90°) - V_{SH}(0°)}{V_{SH}(0°)} = \frac{V_{S1} - V_{S2}}{V_{S2}} = \frac{V_{s\_y} - V_{S\_x}}{V_{S\_x}} \tag{7}$$

Table 1 Bulk density, total porosity, dynamic Young's modulus, static Young's modulus, acoustic impedance, shear impedance, and LMR (lambda–rho and mu–rho) values obtained from physical, mechanical, and ultrasonic tests conducted on core samples

| Sample No	Depth (m)	Density (g/cm^3)	Porosity (%)	Dynamic Young's modulus (GPa)	Static Young's modulus (GPa)	Acoustic impedance (km/s×g/cm^3)	Shear impedance (km/s×g/cm^3)	Lambda–Rho (GPa×g/cm^3)	Mu–Rho (GPa×g/cm^3)
1	2805	2.57	13.20	41.91	12.40	12.32	6.40	71.02	41.00
2	2868	2.57	11.70	39.39	11.94	12.50	6.14	79.62	37.67
3	2921	2.60	15.60	38.02	10.70	11.36	6.19	54.90	38.27
4	2935	2.66	7.25	48.52	17.16	14.46	6.91	111.77	47.73
5	2939	2.54	11.20	40.84	11.36	12.38	6.25	76.88	39.01
6	2942	2.56	16.09	42.83	14.85	11.88	6.54	51.72	42.74
7	2946	2.51	18.03	41.88	10.48	12.16	6.32	69.41	39.97
8	2950	2.42	17.11	32.34	8.32	10.26	5.49	44.21	30.11
9	2954	2.38	17.08	31.30	5.27	10.38	5.31	52.50	28.15
10	2957	2.43	18.71	35.31	10.29	11.17	5.69	59.49	32.38
11	2972	2.47	18.10	33.90	11.89	11.15	5.61	60.91	31.46
12	2890	2.44	17.02	26.83	5.00	10.62	4.90	64.87	23.99
13	2982	2.49	12.65	39.04	13.95	11.83	6.06	67.00	36.77
14	2828	2.54	13.84	44.28	12.78	12.25	6.58	63.55	43.35
15	2987	2.51	15.62	40.81	9.79	11.62	6.29	57.93	39.62
16	2985	2.55	8.78	45.19	15.72	12.44	6.66	68.75	44.35
17	2989	2.63	6.31	48.73	16.62	14.43	6.88	113.99	47.35
18	2995	2.53	9.80	48.20	13.72	12.92	6.84	72.64	46.72
19	3010	2.52	12.93	43.89	14.04	11.58	6.64	46.62	44.04
20	3015	2.53	11.68	39.58	9.90	12.03	6.15	68.47	37.84
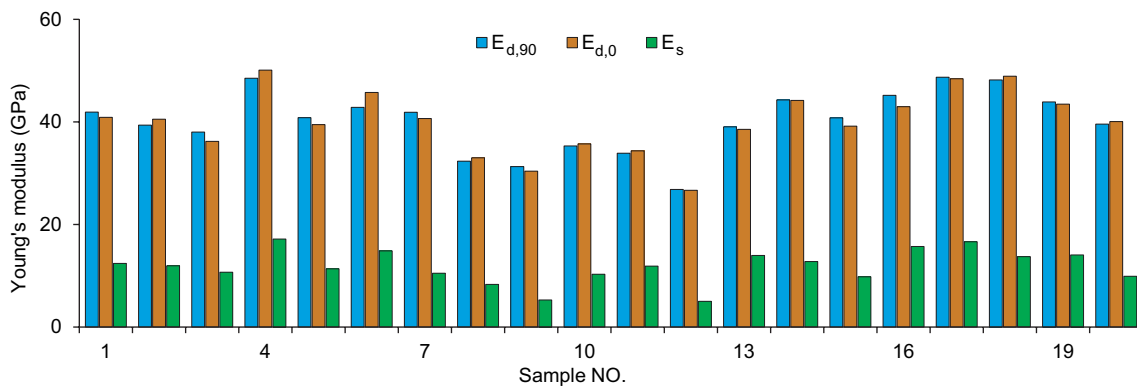
Fig. 7 Plots of static Young's modulus (E_s) and dynamic Young's modulus (E_d) were obtained from the triaxial deformation test and ultrasonic technique, respectively. Also, polarization components of dynamic Young's modulus in horizontal ($E_{d,90}°$) and vertical directions ($E_{d,0}°$) to the axis of symmetry are shown
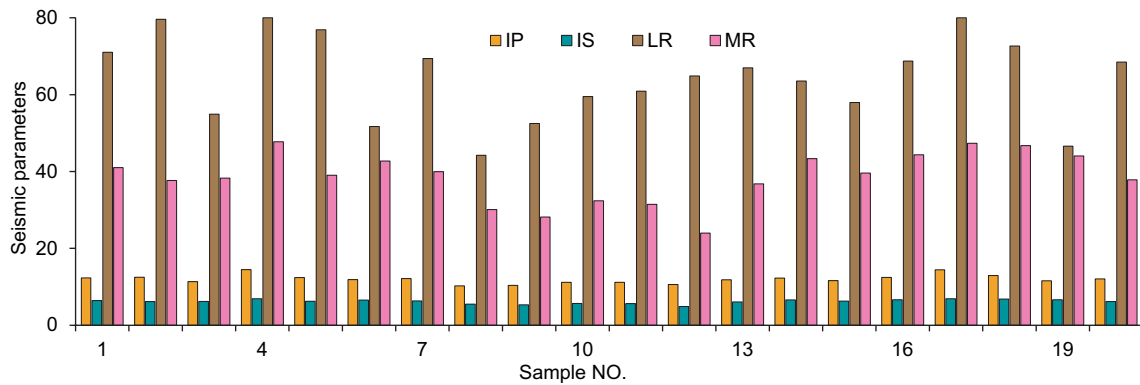
Fig. 8 Values of acoustic and shear impedance (I_p and I_s), lambda–rho (LR), and mu–rho (MR) were obtained from the ultrasonic technique. The shear-wave velocity is obtained by taking the average value over the polarized components
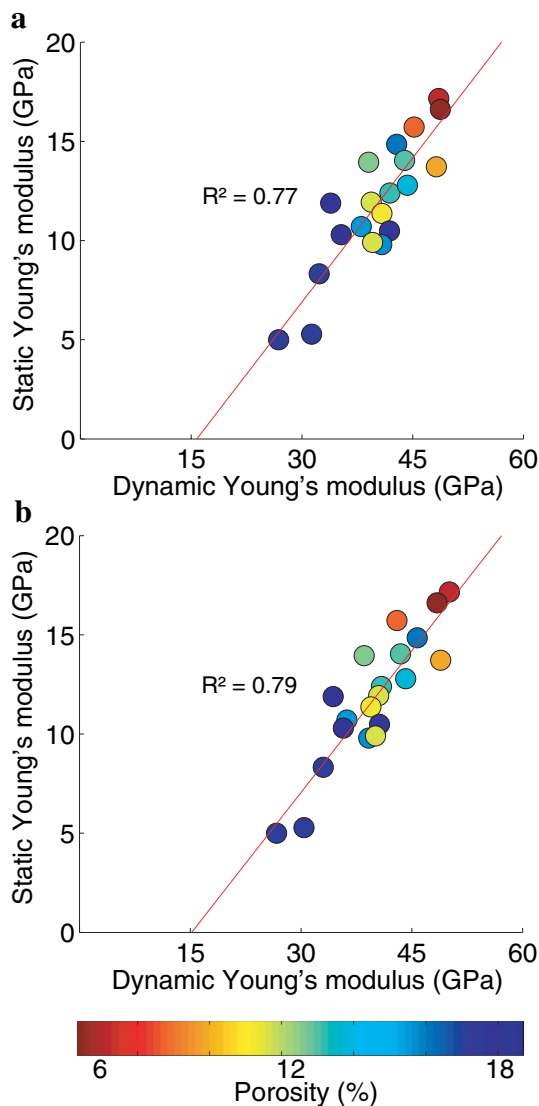

Fig. 9 Cross-plots of static Young's modulus versus dynamic Young's modulus were obtained at **a** vertical and **b** horizontal polarized components of the shear waves, respectively. The coefficient of linear regression is also indicated in the plots. The color bar shows measured porosity (%)

where $V_{SH}(90°)$, Vs_1, and V_{s_y} are velocities of the shear waves polarized along the x-axis. Also, $V_{SH}(0°)$, Vs_2, and V_{s_x} denote the velocities of the shear waves polarized along the y-axis.

Results

Sample characterization

Scanning electron microscope (SEM) images of the studied thin sections exhibited different porosity types, including microcracks, intra-fossil porosity, intra-grain microporosity, and inter-grain porosity. The inter-particle porosity was the dominant pore type in the studied samples. The corresponding microfacies were mudstone to wackestone. In addition, pyritization and dolomitization were observed in the samples. The XRD analysis indicated that the clay contents were predominately composed of kaolinite and illite, along with minor amounts of montmorillonite and sepiolite. Illite fractions were also identified in both heated and non-heated samples, although the corresponding peak to illite could be identified more clearly in the heated samples. Results of the sample characterization (porosity and density) for each core plug are presented in Table 1.

Static and dynamic Young's moduli

In the previous section, rock mechanics tests were conducted on selected samples under drained conditions, and static Young's modulus was measured at in situ confining pressures (Fig. 7). The figure further shows the results of acoustic wave velocity measurements (V_p, V_{s1}, and V_{s2}) on selected samples upon conversion to Young's modulus using elasticity theory. As expected, dynamic Young's

modulus is greater than the static one (e.g., King 1983; Eissa and Kazi 1988). The dynamic Young's modulus increased with increasing the effective confining pressure, possibly due to the closure of microcracks and reduction of porosity followed by water extraction from saturated samples, as reported by Fei et al. (2016). Figure 7 further shows the dynamic Young's modulus plots obtained from the polarization components of shear velocities in horizontal ($V_{\mathrm{SH90}}{}^{\mathrm{o}}$ or V_{s1}) and vertical ($V_{\mathrm{SH0}}{}^{\mathrm{o}}$ or V_{s2}) directions to the axis of symmetry.

Seismic parameters

Seismic parameters such as I_{p}, I_{s}, and LMR can be obtained using Eqs. 1–6. These can then be correlated with ultrasonic measurement data. Figure 8 shows the values of acoustic and shear impedance on saturated samples. The results indicate that P- and S-impedances are affected by P- and S-wave velocities and largely depend on porosity and effective confining pressure (Sharifi et al. 2019), with the dependence being more evident on the P-impedance curve rather than the S-Impedance curve. Lambda–rho and mu–rho are also presented in Fig. 8.

Analysis and discussion

Analysis of static and dynamic Young's moduli

Figure 9 shows the relationship between the static Young's modulus calculated from triaxial tests and the dynamic Young's modulus derived from the ultrasonic measurements. Dynamic Young's modulus was determined under saturated conditions and reservoir pressure and temperature. Figure 9 shows cross-plots of static Young's modulus versus dynamic Young's modulus obtained using vertical and horizontal polarized components of the shear waves, respectively. The results obtained from the ultrasonic test indicated that the selected samples show low degrees of anisotropy.

Even though the static and dynamic moduli show different values and behaviors, those can be correlated with one another via linear or nonlinear relationships. As a statistical method, linear regression is an approach to modeling the relationship between a scalar response (or dependent variable) and one or more explanatory variables (or independent variables). Such an empirical equation can be used in the relationships for exchanging static and dynamic Young's modulus with one another to extend the applicability of those equations. Despite the broad applicability of the regression model, it is sensitive to sample size and outliers, and it only considers the mean of the dependent variables rather than taking into account the confidence intervals; these can negatively affect the final model. A predictive model should have a low mean square error and a high R-squared value (Rawlings 1998; Sharifi et al. 2021). Furthermore, it should pass t- and F-tests with appropriate p-values. To overcome this problem, the analysis of variance (ANOVA) was employed to analyze the results as variable groups were available. ANOVA generalizes the t-test for two groups of variables and compares the groups in terms of their mean values. ANOVA evaluates the mean square, the sum of squares, t-test, and p-values of regression models (Rawlings 1998; Bhattacharya and

Table 2 A summary of ANOVA

Model	Sum of Squares	R-squared	d_{f}	Mean square	F	Sig.
1						
Regression	156.301		1	156.301	57.335	0.009[a]
Residual	49.070	0.761	18	2.726		
Total	205.371		19			
2						
Regression	159.736		2	79.868	29.753	0.002[b]
Residual	45.635	0.778	17	2.684		
Total	205.371		19			
3						
Regression	159.974		3	53.325	18.794	0.006[c]
Residual	45.398	0.779	16	2.837		
Total	205.371		19			

The dependent variable is static Young's modulus (E_{s}). The three models used in this study are presented. The d_{f} is the degree of freedom, F indicates F-value, and sig is the p-value. R-squared is also reported

[a]Predictors: (Constant), E_{d} ($E_{\mathrm{s}} = 0.485 E_{\mathrm{d}} - 7.651$)

[b]Predictors: (Constant), E_{d}, ρ ($E_{\mathrm{s}} = 0.392 E_{\mathrm{d}} + 9.894\rho - 28.866$)

[c]Predictors: (Constant), E_{d}, ρ, ϕ ($E_{\mathrm{s}} = 0.377 E_{\mathrm{d}} + 8.997\rho - 0.049\phi - 25.347$)

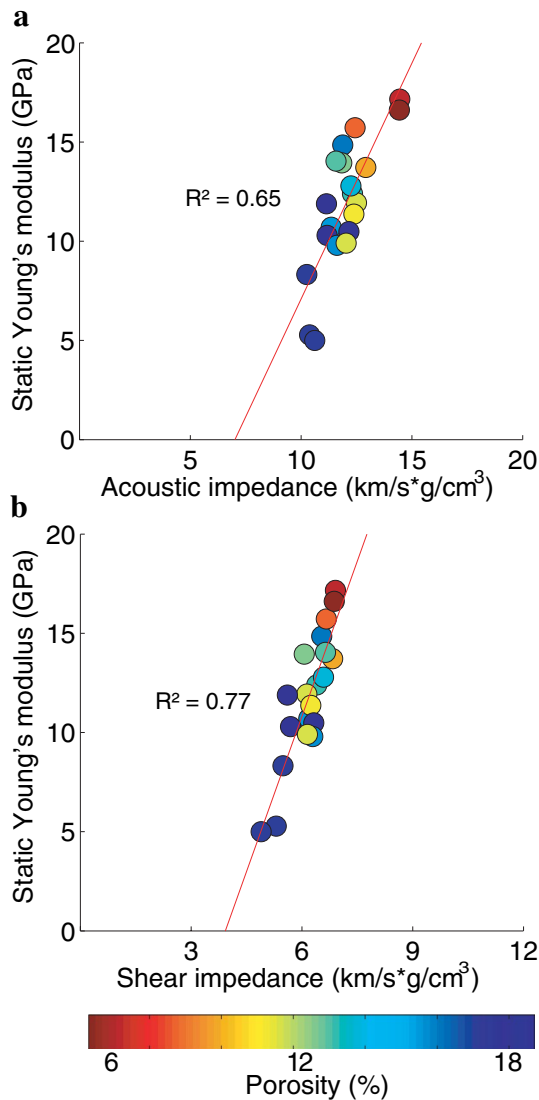**Fig. 10** Cross-plots of static Young's modulus versus **a** acoustic impedance and **b** shear impedance (in km/s.g/cm^3). The color bar refers to porosity (%). The value of the linear regression coefficient is further indicated. Herein shear-wave velocity is obtained by taking the average value over the polarized components

Fig. 11 The relationship between static Young's modulus, on the one hand, and lambda–rho (LR) and mu–rho (MR), on the other hand. Herein shear-wave velocity is obtained by taking the average value over the polarized components. The red line represents the linear regression equation, and the color bar refers to the porosity (%)

Burman 2016). In the presented research, the ANOVA led to the following linear relationship between the dynamic and static Young's moduli at reservoir conditions:

$$E_s = 0.485E_d - 7.651 \tag{8}$$

where E_s and E_d are the static and dynamic Young's moduli in GPa, respectively.

Results of the ANOVA (Table 2, model 1) indicated an appropriate correlation of the static and dynamic Young's moduli ($R^2 = 0.761$), implying adequate accuracy of the model. In order to increase the validity and accuracy of the proposed equation, one must consider more than one
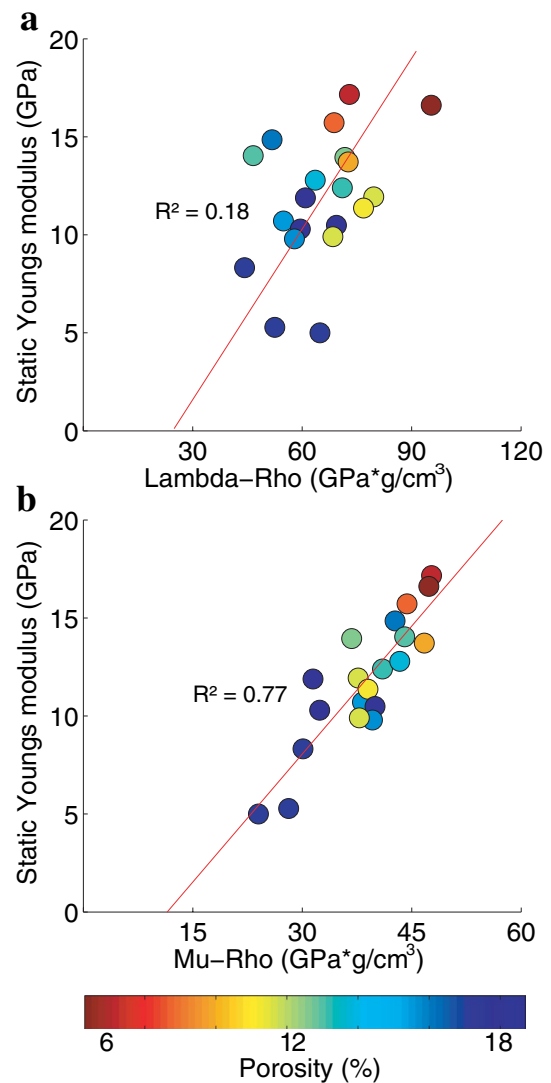
independent variable in the mentioned relationship. In this regard, multivariate regression can be used to consider other independent variables for estimating the static Young's modulus by fitting a straight line to the data. To take this into account, several independent variables (e.g., dynamic Young's modulus, density) were incorporated into the model, and the outcome was analyzed. These independent parameters were chosen because of their availability and ease of determination via routine seismic inversion. In the first stage, the relationships between static Young's modulus and the independent parameters were modeled by introducing the dynamic Young's modulus and density (ρ) information as follows:

$$E_s = 0.392E_d + 9.894\rho - 28.866 \qquad (9)$$

where Young's modulus in GPa and ρ in g/cm^3.

Statistical analysis of the regression parameters led to a correlation coefficient (R^2) of about 0.778. Next, the multivariate regression analysis was continued by adding the porosity (ϕ) to the model, leading to the following equation:

$$E_s = 0.377E_d + 8.997\rho - .049\phi - 25.347 \qquad (10)$$

where Young's modulus in GPa, ρ in g/cm^3, and ϕ is porosity in percent.

Upon statistical evaluations, it was found that a maximum correlation coefficient (R^2) of 0.779 could be achieved by adding more parameters to the model. It can be observed that adding porosity as another variable does not significantly impact the regression correction coefficient. Table 2 summarizes the result of ANOVA for current models, which shows that depending on the regression coefficient and availability of the input variables (e.g., density and porosity), one of these equations can be selected for converting the dynamic modulus to the static Young's modulus.

Analysis of seismic parameters

Seismic parameters were analyzed and plotted against static Young's modulus to perform seismic–geomechanics modeling, as shown in Fig. 10. The results show an excellent agreement between static Young's modulus and either P-impedance or S-impedance. Therefore, these cross-plots provide proper tools for estimating Young's modulus from

Table 3 A summary of ANOVA

Model	Sum of squares	R-squared	d_f	Mean square	F	Sig.
1						
Regression	131.862		1	131.862	32.289	0.004[a]
Residual	73.509	0.642	18	4.084		
Total	205.371		19			
2						
Regression	132.365		2	66.182	15.411	0.013[b]
Residual	73.007	0.645	17	4.295		
Total	205.371		19			
3						
Regression	156.215		1	156.215	57.203	0.000[c]
Residual	49.156	0.761	18	2.731		
Total	205.371		19			
4						
Regression	158.970		2	79.485	29.121	0.088[d]
Residual	46.401	0.774	17	2.729		
Total	205.371		19			
5						
Regression	156.599		1	156.599	57.795	0.039[e]
Residual	48.772	0.763	18	2.710		
Total	205.371		19			
6						
Regression	158.612		2	79.306	28.833	0.817[f]
Residual	46.759	0.772	17	2.751		
Total	205.371		19			

Herein the dependent variable is static Young's modulus (E_s). Details of the six models developed in this research are reported. d_f denotes the degree of freedom, F indicates F-value, and sig is the p-value. R-squared is also reported

[a]Predictors: (Constant), I_p ($E_s = 2.378I_p - 16.695$)

[b]Predictors: (Constant), I_p, ϕ ($E_s = 2.138I_p - 0.084\phi - 12.683$)

[c]Predictors: (Constant), I_s, ($E_s = 5.223I_s - 20.537$)

[d]Predictors: (Constant), I_s, ϕ ($E_s = 4.502I_s - 0.148\phi - 14.052$)

[e]Predictors: (Constant), M_R ($E_s = .435M_R - 5.006$)

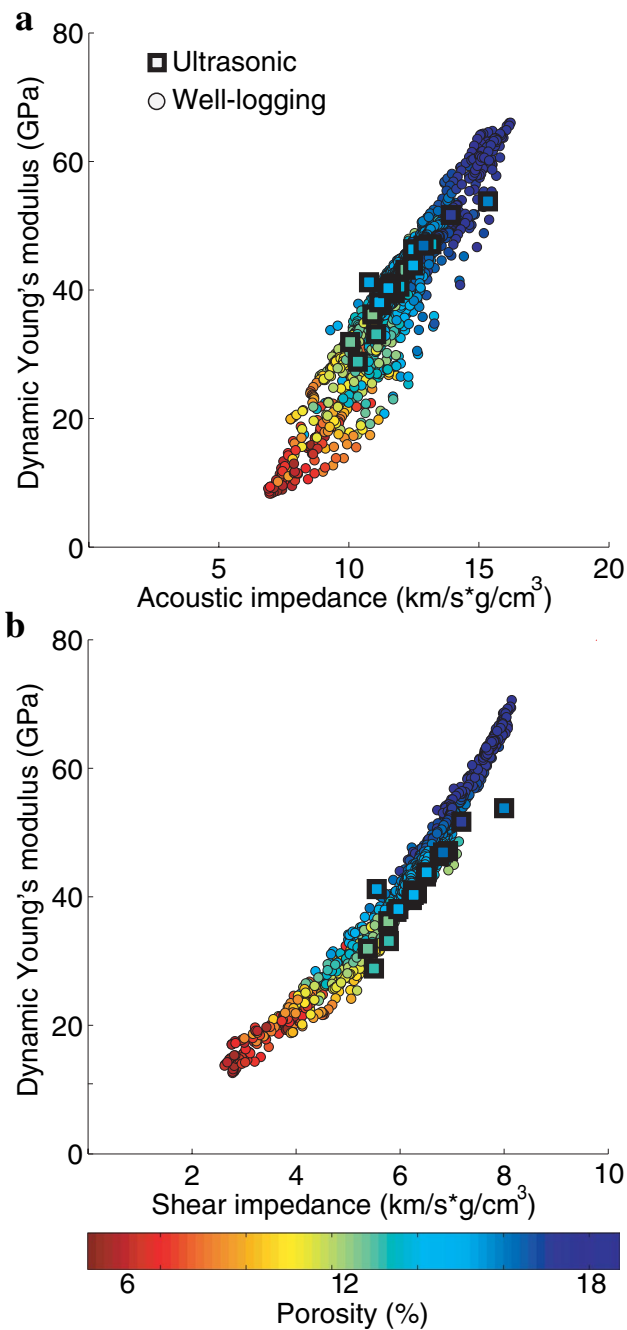[f]Predictors: (Constant), M_R, ϕ ($E_s = .382M_R - .129\phi - 1.177$)

Fig. 12 Cross-plots of dynamic Young's modulus versus **a** acoustic impedance and **b** shear impedance were obtained from the well logging data. The square symbols mark ultrasonic measurements carried out with the reservoir fluid under an effective confining pressure of 40 MPa. Color bar refers to well logging and laboratory-measured porosity (%)

Fig. 13 Well logging data at the selected interval. Track 1 shows measured dynamic Young's modulus (E_d) compared with blind ultrasonic data on core samples. Track 2 denotes the estimated static Young's modulus (E_s) and measured static Young's modulus (using triaxial cell). Track 3 presents the interpreted lithology
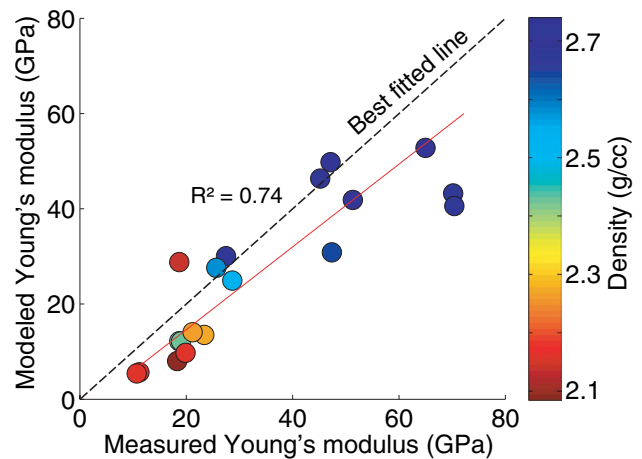

Fig. 14 Results of the blind tests to evaluate the proposed static–dynamic relationships on data from the literature (Van Heerden 1987; Amiri et al. 2019a) for different rock types. The new datasets were not considered when configuring the proposed relationships. The color bar refers to the density (g/cm³), and the red line represents the linear regression equation

the output of seismic inversion for seismic–geomechanics studies.

In addition, Fig. 11 represents the relationship between static Young's modulus, on the one hand, and lambda–rho and mu–rho from ultrasonic measurements, on the other

hand. Some scattering can be seen on the plots, especially when it comes to lambda.

Accordingly, Eq. 11 expresses this relationship between the P-impedance and static Young's modulus:

$$E_s = 2.378I_p - 16.695 \qquad (11)$$

where E_s is the static Young's modulus in GPa and I_p is P-impedance km/s×g/cm^3.

Similarly, static Young's modulus can be related to S-impedance (I_s) via a simple regression equation.

$$E_s = 5.223I_s - 20.537 \qquad (12)$$

where E_s is the static Young's modulus in GPa and I_p is P-impedance km/s×g/cm^3.

A simple regression equation can relate static Young's modulus to mu–rho, as follows:

$$E_s = 0.435M_R - 5.006 \qquad (13)$$

where M_R is the mu–rho in GPa×g/cm^3.

The model of lambda–rho showed a low R-squared value despite a p-value less than 0.05. Therefore, it cannot be a good representative model for our dataset, and hence we removed it from the rest of the analyses. Details of ANOVA are shown in Table 3. The linear multivariate regression analysis results show that depending on the regression coefficient and availability of the dependent (e.g., impedances or LMR) and independent variables (e.g., porosity), one of these equations can be used to convert the seismic parameters to the static Young's modulus.

Analysis of well logging data

Before using well logging data in seismic–geomechanics and inversion applications, one must know how static Young's modulus is correlated with the seismic parameters obtained from the well logs. As core samples may provide solely discrete measurements, well logging is preferred when continuous rock properties are concerned. In situ stress was estimated at the corresponding core depths to select well log values corresponding to those measured on core samples. Then, core properties were shown along with the selected interval. In this regard, Fig. 12 presents cross-plots of the acoustic and shear impedances extracted from the well logs versus dynamic Young's modulus obtained using ultrasonic measurements. It can be seen that the estimated values of dynamic Young's modulus from ultrasonic measurements and well logs agree well with one another. The results also show that the dynamic Young's modulus correlates well with the impedance from well logs.

Using the obtained equation (Eq. 8), the dynamic Young's modulus obtained from well logging was converted to static Young's modulus. Results of evaluating the dynamic and static Young's moduli on the core samples using the ultrasonic technique are shown in Fig. 13. The figure indicates a good agreement between the estimated Young's modulus and the measured values using core data. It also depicts that static and dynamic moduli follow similar trends, although dynamic values are generally greater than static ones.

Differences between the measured and estimated values could be attributed to the uncertainty of dynamic-to–static relationships, depth matching, wellbore instability, anisotropy, and the uncertainty associated with the laboratory tests (ultrasonic and triaxial deformation test). Observed differences in ultrasonic data might also be related to frequency effect (dispersion) and anisotropy. The presence of shale in the Ilam Formation has made the formation susceptible to anisotropy, washout, and collapse (Rajabi et al. 2010). The massive dolomitization observed in the region might also contribute to the deviation of the estimated results from the measured data. Moreover, such measurements are made along the wellbore axis, which is frequently not perpendicular to the bedding orientation, causing anisotropic effects (Nooraiepour et al. 2017b).

Blind test data

In order to confirm the capability of the obtained relationships, blind tests were performed to quality control the developed equations. A high-accuracy relationship is supposed to yield a good match between the target parameter (Young's modulus) and measured data via a series of blind tests. For the blind tests, the building of the regression model and related analyses were performed without considering a particular set of data (from now on referred to as the blind data). Next, using the respective formula and the developed static–dynamic conversion relationships, the static Young's modulus was estimated using the blind data (Van Heerden 1987; Amiri et al. 2019a). Then, the obtained values were cross-correlated with the measured Young's moduli from the datasets (Fig. 14). The results showed that the estimated values of Young's modulus followed the measured ones, as per the considered datasets. Nevertheless, the lower correlation coefficients obtained in the blind tests might be attributed to the factors affecting the strain rate, strain amplitude, frequency, mineralogy, and pore shape (King 1983; Petrov 2014; Fjær 2019).

Limitations and errors

Acoustic wave velocities and attenuation in fluid-bearing rocks are known to be influenced by two major fluid/solid interaction models: (1) the Biot mechanism, in which viscous friction and inertial coupling make the fluid contribute to the matrix motion, and (2) the squirt-flow mechanism,

in which the deforming impact of the propagating wave on thin pores makes the fluid squeezed out of the pores. Dvorkin and Nur (1993) suggested a model called BISQ (Biot and squirt-flow mechanism), where both mechanisms were treated as coupled processes. In the laboratory, wave velocity was measured at ultrasonic frequencies (typically 500–1000 kHz), while sonic well logs contain velocity information at much lower frequencies (intermediate frequencies). Considering the characteristics of the brine-saturated samples in terms of pore structure, pore fluid, and permeability, the Biot characteristic frequency was found to exceed 1 MHz. Although the Biot approximation seemed unrealistic, focusing on brine-saturated samples, BISQ prediction implied that well logs and corresponding laboratory measurements at ultrasonic frequencies refer to unrelaxed velocity variations. For the brine-saturated samples considered in this study, a Biot characteristic frequency from an order of some kHz was approximated. Therefore, attenuation could be expected in the selected samples, and the frequency could affect velocity measurements (and hence the dynamic parameters). With this approach, one needs to measure values of P-wave and S-wave velocities on saturated rock samples. In many cases, the dispersion ranges from about 10 percent at lower effective stresses to only a few percentages at higher stresses. In this research, considering initial porosity and water saturation and the effective stress applied to the samples, the dispersion of wave velocity measurements based on Winkler (1986) was estimated to be below 5%. In a quasi-static test, the heterogeneities tend to affect the elastic properties. In contrast, in a dynamic test, waves travel through the body of the sample along a direct path or within a particular volume in the sample, avoiding potential discontinuities rather than representing the whole body of the sample. Another vital factor to consider is the wavelength. In ultrasonic tests and well logging methods, given that wavelength of the wave emitted by the tool is much longer than the scale of discontinuities within the investigated formation, the results of the static tests are more scale-dependent than those of the dynamic tests. For the static tests, reducing the size of the core plugs containing microcracks and fissures is likely to represent the static modulus of the intact rock.

Conclusions

In this paper, well logging data and a total of 20 core plugs from a carbonate field were studied to investigate the relationship between static Young's moduli and seismic parameters under reservoir conditions. Our results confirmed that static and dynamic parameters exhibit similar behaviors under the considered confining pressures so that one can link them together through a linear relationship. Analysis of variance (ANOVA) was performed to propose a relationship between static and dynamic Young's moduli considering other rock properties. A more thorough comparison between these relationships showed that the best match with static Young's modulus could be obtained using ultrasonic data such as S-impedance and P-impedance followed by Mu–rho. Furthermore, the present study indicates that laboratory (ultrasonic) measurements are better correlated with static measurements than well logging data due to wellbore instability, anisotropy, and dispersion. In addition, obtained relationships were examined through blind tests in reservoirs far from the initial study location. Results of the blind tests confirmed the reliability of the proposed relationships. The outcomes of the present study may have implications for geomechanical modeling, seismic–geomechanics inversion, and structural modeling/restoration.

Declarations

Conflict of interest The authors declare that there are no known conflicts of interest associated with this research, and there has been no financial support for this work that could have influenced its outcome.

Ethical approval The authors assure that this manuscript manifests original research work that reflects their research analysis in a truthful manner.

References

Amalokwu K, Best AI, Chapman M (2016) Effects of aligned fractures on the response of velocity and attenuation ratios to water saturation variation: a laboratory study using synthetic sandstones. Geophys Prospect 64:942–957. https://doi.org/10.1111/1365-2478.12378

Amiri M, Lashkaripour GR, Ghabezloo S et al (2019a) Mechanical earth modeling and fault reactivation analysis for CO$_2$-enhanced oil recovery in Gachsaran oil field, south-west of Iran. Environ Earth Sci 78:112. https://doi.org/10.1007/s12665-019-8062-1

Amiri M, Lashkaripour GR, Ghabezloo S, Hafezi Moghaddas N, Tajareh MH (2019b) 3D spatial model of Biot's effective stress coefficient using well logs, laboratory experiments, and geostatistical method in the Gachsaran oil field, southwest of Iran. Bull Eng Geol Environ 78(6):4633–4646. https://doi.org/10.1007/s10064-018-1423-2

Anderson EM (1951) The dynamics of faulting and dyke formation with applications to Britain. Oliver and Boyd, Edinburgh

Bhattacharya PK, Burman P (2016) Theory and methods of statistics, Elsevier Inc

Brady BHG, Brown ET (2013) Rock mechanics: for underground mining. Springer Science & Business Media

Brie A, Endo T, Hoyle D, Codazzi D, Esmersoy C, Hsu K et al (1998) New directions in sonic logging. Oilfield Rev 10:14

Brotons V, Tomás R, Ivorra S, Grediaga A (2014) Relationship between static and dynamic elastic modulus of calcarenite heated at different temperatures: the San Julián's stone. Bull Eng Geol Environ 73:791–799. https://doi.org/10.1007/s10064-014-0583-y

Deere DU, Miller RP (1966) Engineering classification and index properties for intact rock

Dvorkin J, Nur A (1993) Dynamic poroelasticity: a unified model with the squirt and the Biot mechanisms. Geophysics 58:524–533

Eissa EA, Kazi A (1988) Relation between static and dynamic Young's moduli of rocks. Int J ROCK Mech Min Geomech Abstr 25

Farrokhrouz M, Asef MR, Kharrat R (2014) Empirical estimation of uniaxial compressive strength of shale formations. Geophysics 79(4):D227–D233. https://doi.org/10.1190/geo2013-0315.1

Fei W, Huiyuan B, Jun Y, Yonghao Z (2016) Correlation of dynamic and static elastic parameters of rock. Electron J Geotech Eng 21:1551–1560

Fjær E (2019) Relations between static and dynamic moduli of sedimentary rocks. Geophys Prospect 67:128–139. https://doi.org/10.1111/1365-2478.12711

Goodman RE (1989) Introduction to rock mechanics. Wiley, New York

Gray D, Anderson P, Logel J, Delbecq F, Schmidt D, Schmid R (2012) Estimation of stress and geomechanical properties using 3D seismic data. First Break 30(3):59–68. https://doi.org/10.3997/1365-2397.2011042

Hamilton EL, Bachman RT (1982) Sound velocity and related properties of marine sediments. J Acoust Soc Am 72:1891–1904

Hampson DP, Russell BH, Bankhead B (2005) Simultaneous inversion of pre-stack seismic data, In: 75th annual international meeting, SEG, Expanded abstracts, pp 1633–1636. https://doi.org/10.1190/1.2148008

Hashiba K, Fukui K (2014) New multi-stage triaxial compression test to investigate the loading-rate dependence of rock strength. Geotech Test J 37:1087–1091. https://doi.org/10.1520/GTJ20140061

Herwanger J, Koutsabeloulis N (2011) Seismic geomechanics: how to build and calibrate geomechanical models using 3D and 4D seismic data. EAGE Publications

Hornby BE (1998) Experimental laboratory determination of the dynamic elastic properties of wet, drained shales. J Geophys Res Solid Earth 103:29945–29964

Ide JM (1936) Comparison of statically and dynamically determined Young's modulus of rocks. Proc Natl Acad Sci U S A 22:81

Jiang Z, Xiong Y (2019) Seismic inversion for fluid bulk modulus based on elastic impedance. J Appl Geophys 169:74–84. https://doi.org/10.1016/j.jappgeo.2019.06.013

Kidambi T, Kumar GS (2016) Mechanical Earth Modeling for a vertical well drilled in a naturally fractured tight carbonate gas reservoir in the Persian Gulf. J Pet Sci Eng 141:38–51. https://doi.org/10.1016/j.petrol.2016.01.003

Kim MM, Ko H-Y (1979) Multistage triaxial testing of rocks. Geotech Test J 2:98–105

King MS (1983) Static and dynamic elastic properties of igneous and metamorphic rocks from the Canadian shield

Lockner D, Byerlee JD, Kuksenko V et al (1991) Quasi-static fault growth and shear fracture energy in granite. Nature 350:39

Mavko G, Mukerji T, Dvorkin J (2009) The rock physics handbook, Second Edition

McCann C, Sothcott J (1992) Laboratory measurements of the seismic properties of sedimentary rocks. Geol Soc London, Spec Publ 65:285–297

Mockovčiaková A, Pandula B (2003) Study of the relation between the static and dynamic moduli of rocks. Metalurgija 42:37–39

Motiei H et al (1993) Stratigraphy of Zagros. Treatise Geol Iran 60:151

Najibi AR, Ghafoori M, Lashkaripour GR, Asef MR (2015) Empirical relations between strength and static and dynamic elastic properties of Asmari and Sarvak limestones, two main oil reservoirs in Iran. J Petrol Sci Eng 126:78–82. https://doi.org/10.1016/j.petrol.2014.12.010

Nooraiepour M, Haile BG, Hellevang H (2017a) Compaction and mechanical strength of middle miocene mudstones in the Norwegian north sea: the major seal for the Skade CO$_2$ storage reservoir. Int J Greenhouse Gas Control 67:49–59. https://doi.org/10.1016/j.ijggc.2017.10.016

Nooraiepour M, Mondol NH, Hellevang H, Bjørlykke K (2017b) Experimental mechanical compaction of reconstituted shale and mudstone aggregates: investigation of petrophysical and acoustic properties of SW Barents Sea cap rock sequences. Mar Petrol Geol 80:265–292. https://doi.org/10.1016/j.marpetgeo.2016.12.003

Petrov A (2014) Static moduli prediction using integration between rock physics and dynamic moduli. In: Second EAGE workshop on rock physics. https://doi.org/10.3997/2214-4609.20132063

Rajabi M, Sherkati S, Bohloli B, Tingay M (2010) Subsurface fracture analysis and determination of in-situ stress direction using FMI logs: an example from the Santonian carbonates (Ilam formation) in the Abadan plain. Iran Tectonophys 492:192–200. https://doi.org/10.1016/j.tecto.2010.06.014

Rawlings JO, Pantula SG, Dickey DA (1998) Applied regression analysis: a research tool, 2nd edn. Springer-Verlag, New York

Saberi MR, Ting J (2016) A workflow to model anisotropy in a vertical transverse isotropic medium. First Break 34:41–48

Sen MK (2006) Seismic inversion: society of petroleum engineers

Serra O (1986) Fundamentals of well-log interpretation (vol. 2): the interpretation of logging data (developments in petroleum science). Elsevier 15, p 679

Sharifi J (2022) Dynamic-to-static modeling. Geophysics 87(2):MR63–MR72. https://doi.org/10.1190/geo2020-0778.1

Sharifi J, Hafezi Moghaddas N et al (2019) Application of extended elastic impedance in seismic geomechanics. Geophysics 84(3):R429–R446. https://doi.org/10.1190/geo2018-0242.1

Sharifi J, Mirzakhanian M (2018) Determination of geomechanical parameters using extended elastic impedance (EEI), In: 80th annual international conference and exhibition, EAGE, extended abstracts, Th_P06_15, https://doi.org/10.3997/2214-4609.20180 1613

Sharifi J, Mirzakhanian M, Javaherian A et al (2017) An investigation on the relationship between static and dynamic bulk modulus on an Iranian oilfield, In: 79th annual international conference and exhibition, EAGE, extended abstracts, Th SP1 08, https://doi.org/10.3997/2214-4609.201701465

Sharifi J, Nooraiepour M, Mondol NH (2021) Application of the analysis of variance for converting dynamic to static Young's modulus, In: 82th annual international conference and exhibition, EAGE, extended abstracts, Th_P01_16, https://doi.org/10.3997/2214-4609.202012000

Thomsen L (1986) Weak elastic anisotropy. Geophysics 51:1954–1966

Ugbor CC, Odong PO, Akpan AS (2021) Application of pre-stack seismic waveform inversion and empirical relationships for the estimation of geomechanical properties in ruby field, central swamp depobelt, Onshore Niger delta, Nigeria. J Petrol

Explor Prod Technol 11:2389–2406. https://doi.org/10.1007/s13202-021-01219-w

Van Heerden WL (1987) General relations between static and dynamic moduli of rocks. Int J ROCK Mech Min Geomech Abstr 24(6):381–385

Winkler KW (1986) Estimates of velocity dispersion between seismic and ultrasonic frequencies. Geophysics 51:183–189

Yin H (1992) Acoustic velocity and attenuation of rocks: isotropy, intrinsic anisotropy, and stress induced anisotropy. Department of Geophysics, School of Earth Sciences, Stanford Univ

Zare-Reisabadi M, Rajabi M, Velayati A, Pourmazaheri Y, Haghighi M (2018) 1D Mechanical earth model in a carbonate reservoir of the abadan plain, southwestern iran: implications for wellbore stability. Paper presented at the AAPG geosciences technology workshop: pore pressure and geomechanics: from exploration to abandonment, Perth, Australia

Zoback MD (2010) Reservoir geomechanics. Cambridge University Press